

Magnetic susceptibility of a strongly interacting thermal medium with $2 + 1$ quark flavors

Kazuhiko Kamikado^a and Takuya Kanazawa^b

^a*Theoretical Research Division, Nishina Center, RIKEN, Wako, Saitama 351-0198, Japan*

^b*Quantum Hadron Physics Laboratory, RIKEN, Wako, Saitama 351-0198, Japan*

E-mail: kazuhiko.kamikado@riken.jp, takuya.kanazawa@riken.jp

ABSTRACT: Thermodynamics of the three-flavor quark-meson model with $U_A(1)$ anomaly is studied in the presence of external magnetic fields. The nonperturbative functional renormalization group is employed in order to incorporate quantum and thermal fluctuations beyond the mean-field approximation. We calculate the magnetic susceptibility with proper renormalization and find that the system is diamagnetic in the hadron phase and paramagnetic in the hot plasma phase. The obtained values of the magnetic susceptibility are in reasonable agreement with the data from first-principle lattice QCD. Comparison with the mean-field approximation, the Hadron Resonance Gas model and a free gas with temperature-dependent masses is also made.

Contents

1	Introduction	1
2	Formulation	3
2.1	$N_f = 3$ Quark-Meson model	3
2.2	Functional renormalization group equation	4
2.3	Observables	6
3	Numerical implementation	7
3.1	Setup	7
3.2	Results at nonzero magnetic field	9
3.2.1	Pressure, masses and decay constants	9
3.2.2	Magnetic susceptibility	11
4	Conclusions and outlook	13
A	Summary of the $N_f = 2$ QM model	14
B	Mass spectrum in the $N_f = 3$ QM model	15
C	Taylor method	17
C.1	Two flavors	17
C.2	Three flavors	18
D	Magnetic susceptibility of a non-interacting quark-meson gas	19
D.1	Quarks	21
D.2	Mesons	22

1 Introduction

Recent years have seen a surge of interest in QCD in external magnetic fields. The electromagnetic response of QCD is not only interesting as a theoretical probe to the dynamics of QCD, but also important in experimental heavy ion collisions, cosmology and astrophysics. Special neutron stars called magnetars possess a strong surface magnetic field reaching 10^{10} T [1, 2] whereas the primordial magnetic field in early Universe is estimated to be even as large as $\sim 10^{19}$ T [3]. In non-central heavy ion collisions at RHIC and LHC, an instantaneous magnetic field of strength $\sim 10^{15}$ T perpendicular to the reaction plane could be produced and may have impact on the thermodynamics of the quark-gluon plasma, which could lead to experimentally useful signatures [4–6].

The effect of magnetic field on the chiral dynamics of QCD at finite temperature $T > 0$ has been vigorously investigated in chiral effective models (see [7, 8] for reviews). Among other things it was found that the magnetic field catalyzes spontaneous chiral symmetry breaking at least for low T , an effect called *magnetic catalysis*. This model-independent phenomenon is explained through dimensional reduction ($3+1 \rightarrow 1+1$) in the quark sector in a magnetic field [9, 10]. The dynamics of QCD in a magnetic field has also been studied in lattice simulations [11–25], see [26] for a review. Simulations at the physical quark mass [15, 18] showed that the effect of a magnetic field is non-monotonic: although the chiral condensate increases at low temperature, it *decreases* at high temperature, resulting in a lower chiral pseudo-critical temperature T_c in a stronger magnetic field. Gluonic observables also show a similar behavior [20]. Various attempts have been made to explain the origin of this *inverse magnetic catalysis*¹ (or *magnetic inhibition*) [29–41].

Lattice measurements of quantities such as the pressure, energy density, entropy density and magnetization have revealed thermodynamic properties of QCD in external magnetic fields. In particular, the *magnetic susceptibility*² $\chi(T)$, which quantifies the leading response of pressure to weak external magnetic fields, has been accurately measured in recent lattice simulations with light dynamical quarks [21, 22, 24, 45, 46], where various methods were adopted to circumvent the flux quantization condition on a periodic lattice, as summarized in [46, Sec. 3.1]. The simulations revealed that QCD at $T \gtrsim T_c$ is strongly *paramagnetic*, characterized by $\chi > 0$, whereas the behavior at $T \lesssim 100$ MeV is consistent with *weak diamagnetism* with $\chi \lesssim 0$. Thus, interestingly, QCD seems to undergo a characteristic change in its magnetic profile at finite temperature, despite the absence of a genuine phase transition. On the theoretical side, the magnetization and magnetic susceptibility of QCD at zero density have been studied in, e.g., perturbative QCD [47], the Hadron Resonance Gas model [48], holographic QCD [49], a transport model [50], a potential model [51], a non-interacting quark gas with the Polyakov loop [52], spatially compactified QCD [53] and the SU(3) linear sigma model with the Polyakov loop [54].

In this work, we apply the functional renormalization group (FRG) [55] to the quark-meson (QM) model with three quark flavors to study magnetic properties of QCD at finite temperature and zero density. FRG is a powerful nonperturbative method to go beyond the mean-field approximation by fully taking thermal and quantum fluctuations into account; see [56–59] for reviews. While FRG has already been applied to chiral models in a magnetic field [35, 60–64], so far no attempt has been made to include strangeness. Here we shall extend the FRG analysis of the $N_f = 3$ QM model [65] to the case of nonzero magnetic fields and study its thermodynamic behavior, with particular emphasis on the magnetic susceptibility, $\chi(T)$.

¹There is a similar phenomenon called by the same name but is specific to nonzero chemical potential [27]. This seems to have a different origin from that of inverse magnetic catalysis at zero density; the interested reader is referred to a review [28].

²To avoid confusion, we remark that a quantity called *magnetic susceptibility of the quark condensate* is defined with regard to the tensor polarization $\langle \bar{\psi} \sigma_{\mu\nu} \psi \rangle$ [42] and has been measured on the lattice [19, 43] (for theoretical works, see [44] and references therein). However, this “susceptibility” is just the spin-related piece of the full magnetic susceptibility defined from the pressure in a magnetic field. In this paper we focus on the latter *full* magnetic susceptibility, not the former.

While it seems well recognized by now that chiral effective models do not support the inverse magnetic catalysis of QCD in a *strong* magnetic field, it does not necessarily imply that they also fail to explain the behavior of QCD in a *weak* magnetic field. Refs. [36, 37, 40] suggest that the running of the QCD coupling with a magnetic field could be the origin of the inverse magnetic catalysis, but such a factor is not likely to play a dominant role in QCD in an infinitesimal magnetic field. This line of reasoning leaves open the possibility that chiral models may be able to capture physics at weak external fields correctly. Our aim is to put this expectation to the test through a stringent quantitative comparison between lattice data and the FRG calculation.

This paper is organized as follows. In section 2, we introduce the $N_f = 3$ QM model and describe the formulation of FRG. We specify our truncation of the scale-dependent quantum effective action, introduce regulator functions and present the flow equation. In section 3, we show plots of physical observables obtained by solving the flow equation numerically and discuss their characteristics. The main results are summarized in Figures 4 and 5. We compare the magnetic susceptibility from $N_f = 3$ FRG with results from recent lattice simulations, $N_f = 2$ FRG, the mean-field calculation, and non-interacting quark-meson gas with temperature-dependent masses. Section 4 is devoted to conclusions. Technical details of the flow equation and the derivation of pressure of a non-interacting gas are relegated to the appendices.

In this paper we will use natural units and the Heaviside-Lorentz conventions, in which $\varepsilon_0 = \mu_0 = 1$ and the fine-structure constant $\alpha_{\text{em}} = e^2/4\pi \approx 1/137$. The magnitude of a magnetic field \mathbf{B} will be measured in the combination eB , which is useful in natural units.

2 Formulation

In Section 2.1 we introduce the three-flavor QM model as an effective model with the same chiral symmetry breaking pattern as in QCD. In Section 2.2 we review basics of FRG and explain how mesonic fluctuations which are neglected in the mean-field approximation are incorporated by the non-perturbative flow equation. Finally in Section 2.3, we explain how to compute observables from the effective potential of the model.

2.1 $N_f = 3$ Quark-Meson model

The $N_f = 3$ QM model [54, 65–73] is the U(3) linear sigma model [74–82] coupled to quarks:

$$\begin{aligned} \mathcal{L} = & \sum_{i=1}^{N_c} \bar{\psi}_i \left[\not{D} + g \sum_{a=0}^8 T_a (\sigma_a + i\gamma_5 \pi_a) \right] \psi_i + \text{tr} [\mathcal{D}_\mu \Sigma (\mathcal{D}_\mu \Sigma)^\dagger] \\ & + U(\rho_1, \rho_2) - h_x \sigma_x - h_y \sigma_y - c_A \xi. \end{aligned} \quad (2.1)$$

Several remarks are in order.

- $\psi = (u, d, s)^T$ represents the three-flavor quark field with three colors ($N_c = 3$).
- Σ is a matrix field consisting of the scalar (σ_a) and pseudo-scalar (π_a) meson multiplets,

$$\Sigma = \sum_{a=0}^8 T_a (\sigma_a + i\pi_a), \quad (2.2)$$

where $\{T_a\}$ are the nine generators of $U(3)$ normalized as $\text{tr}[T_a T_b] = \frac{1}{2}\delta_{ab}$. They are related to the Gell-Mann matrices as $T_a = \lambda_a/2$ ($a = 1, \dots, 8$), and $T_0 = \mathbb{1}/\sqrt{6}$.

- The covariant derivatives are defined as

$$\mathcal{D} \equiv \gamma_\mu (\partial_\mu - iQ A_\mu) \quad \text{and} \quad \mathcal{D}_\mu \Sigma \equiv \partial_\mu \Sigma - iA_\mu [Q, \Sigma], \quad (2.3)$$

with $Q = \text{diag} \left(\frac{2}{3}e, -\frac{1}{3}e, -\frac{1}{3}e \right)$, $\vec{A} = (0, Bx_1, 0)$ and $A_4 = 0$.

- $U(\rho_1, \rho_2)$ is the $U(3) \times U(3)$ -invariant part of the bosonic potential written in terms of two invariants³

$$\rho_1 = \text{tr}[\Sigma \Sigma^\dagger] \quad \text{and} \quad \rho_2 = \text{tr} \left[\left(\Sigma \Sigma^\dagger - \frac{1}{3} \rho_1 \mathbb{1} \right)^2 \right]. \quad (2.4)$$

By definition, $\rho_1 \geq 0$ and $\rho_2 \geq 0$. In this work we neglect the possible dependence of U on another invariant $\text{tr}[(\Sigma \Sigma^\dagger)^3]$ for simplicity.⁴

- The linear terms $h_x \sigma_x + h_y \sigma_y$ stand for the explicit chiral symmetry breaking due to nonzero quark masses. The strange-nonstrange basis is defined as

$$\begin{pmatrix} \sigma_x \\ \sigma_y \end{pmatrix} \equiv \frac{1}{\sqrt{3}} \begin{pmatrix} \sqrt{2} & 1 \\ 1 & -\sqrt{2} \end{pmatrix} \begin{pmatrix} \sigma_0 \\ \sigma_8 \end{pmatrix}. \quad (2.5)$$

This parametrization automatically respects the $SU(2)_V$ symmetry of light quarks.

- $\xi \equiv \det \Sigma + \det \Sigma^\dagger$ represents the effect of the $U_A(1)$ anomaly. Another invariant $i(\det \Sigma - \det \Sigma^\dagger)$ breaks CP invariance of the model and is omitted.

2.2 Functional renormalization group equation

The basic idea of FRG is to start from a tree-level classical action $\Gamma_{k=\Lambda}$ at the UV scale Λ , and keep track of the flow of the scale-dependent effective action Γ_k while integrating out degrees of freedom with intermediate momenta successively; finally at $k = 0$ the full quantum effective action $\Gamma_{k=0}$ is obtained. The functional renormalization group equation [55] (called the Wetterich equation) reads

$$\partial_k \Gamma_k = \frac{1}{2} \text{Tr} \left[\frac{1}{\Gamma_k^{(2,0)} + R_k^B} \partial_k R_k^B \right] - \text{Tr} \left[\frac{1}{\Gamma_k^{(0,2)} + R_k^F} \partial_k R_k^F \right], \quad (2.6)$$

where R_k^B and R_k^F are cutoff functions (regulators) for bosons and fermions, while $\Gamma_k^{(2,0)}$ and $\Gamma_k^{(0,2)}$ represent the second functional derivative of Γ_k with respect to bosonic and fermionic fields, respectively. Tr is a trace in the functional space. Although (2.6) has a simple one-loop structure, (2.6) incorporates effects of arbitrarily high order diagrams in the perturbative expansion through the full field-dependent propagator $(\Gamma_k^{(2)} + R_k)^{-1}$. Further details of FRG can be found in reviews [56–59].

³To avoid confusion, we note that our ρ_2 defined in (2.4) coincides with $\tilde{\rho}_2$ in [65].

⁴Generally, we have N independent invariants for $U(N) \times U(N)$ chiral flavor rotation [66].

The flow of Γ_k from UV to IR is governed by the cutoff functions $R_k^{B,F}(p)$. The latter must satisfy (i) $\lim_{k \rightarrow \infty} R_k(p) = \infty$, (ii) $\lim_{k \rightarrow 0} R_k(p) = 0$, and (iii) $\lim_{p \rightarrow 0} R_k(p) > 0$ [56]. In this work we use the following regulators

$$R_k^B(p) = (k^2 - \vec{p}^2) \Theta(k^2 - \vec{p}^2), \quad (2.7a)$$

$$R_k^F(p) = -i \vec{p} \vec{r}_k(\vec{p}) \quad \text{with} \quad r_k(\vec{p}) \equiv \left(\frac{k}{|\vec{p}|} - 1 \right) \Theta(k^2 - \vec{p}^2), \quad (2.7b)$$

for bosons and fermions, respectively. These are the finite-temperature version of the so-called optimised regulator [83]. They can be used in a magnetic field as well [63]. With this choice of regulators, we can perform the Matsubara sum analytically.

Although the Wetterich equation (2.6) formulated in the infinite-dimensional functional space is *exact*, for practical calculations we must find a proper truncation of Γ_k . In this work we employ the so-called local-potential approximation (LPA), which neglects anomalous dimensions of fields altogether but is commonly used due to its technical simplicity. More explicitly, we use the truncated effective action at the scale k of the form

$$\begin{aligned} \Gamma_k[\psi, \sigma, \pi] = & \int_0^{1/T} dx_4 \int d^3x \left\{ \sum_{i=1}^{N_c} \bar{\psi}_i \left[\not{D} + g \sum_{a=0}^8 T_a(\sigma_a + i\gamma_5 \pi_a) \right] \psi_i \right. \\ & \left. + \text{tr} [(\mathcal{D}_\mu \Sigma)(\mathcal{D}_\mu \Sigma)^\dagger] + U_k(\rho_1, \rho_2) - h_x \sigma_x - h_y \sigma_y - c_A \xi \right\}. \end{aligned} \quad (2.8)$$

Here, for a technical reason, we have ignored isospin symmetry breaking in the bosonic potential due to the magnetic field (see also [64] for a discussion on this point). In the limit $B \rightarrow 0$, (2.8) reduces to the effective action used in [65].

By using the cutoff functions (2.7a), (2.7b), and the LPA effective action (2.8), we can easily derive the flow equation for the symmetric part of the bosonic potential [60, 63, 64]:

$$\partial_k U_k = \frac{k^4}{12\pi^2} \left\{ \sum_b \alpha_b(k) \frac{\coth \frac{E_b(k)}{2T}}{E_b(k)} - \sum_{f=u,d,s} \alpha_f(k) \frac{\tanh \frac{E_f(k)}{2T}}{E_f(k)} \right\}, \quad (2.9)$$

where the index b runs over all $9 + 9 = 18$ mesons. $E_b(k)$ and $E_f(k)$ are scale- and field-dependent energies of mesons and fermions, respectively, defined as $E_i(k) \equiv \sqrt{k^2 + M_i^2}$. For quarks, we have

$$M_{u,d} = \frac{g\sigma_x}{2} \quad \text{and} \quad M_s = \frac{g\sigma_y}{\sqrt{2}}. \quad (2.10)$$

The meson masses are summarized in appendix B.

The dimensionless factors $\alpha_b(k)$ and $\alpha_f(k)$ are defined as

$$\alpha_b(k) = 3 \frac{|e_b B|}{k^2} \sum_{n=0}^{\infty} \sqrt{1 - (2n+1) \frac{|e_b B|}{k^2}} \Theta \left(1 - (2n+1) \frac{|e_b B|}{k^2} \right), \quad (2.11a)$$

$$\alpha_f(k) = 6N_c \frac{|e_f B|}{k^2} \left\{ 1 + 2 \sum_{n=1}^{\infty} \sqrt{1 - 2n \frac{|e_f B|}{k^2}} \Theta \left(1 - 2n \frac{|e_f B|}{k^2} \right) \right\}, \quad (2.11b)$$

where e_b and e_f are the electric charge of each field. For neutral particles ($e_b, e_f = 0$), or for charged particles in the limit of a vanishing magnetic field ($eB \rightarrow 0$), these factors simply become $\alpha_b(k) = 1$ and $\alpha_f(k) = 4N_c$, which recovers the conventional flow equation in the absence of magnetic fields correctly [63].

2.3 Observables

Let us explain how to obtain physical quantities from the $k \rightarrow 0$ limit of the flow equation. First of all, the condensates are determined from the minimum of the total effective potential at $k = 0$. We denote the expectation values of σ_x and σ_y thus obtained as $\langle \sigma_x \rangle_{k=0}$ and $\langle \sigma_y \rangle_{k=0}$, respectively. The physical constituent quark masses are obtained from (2.10) as

$$M_{u,d} = \frac{g}{2} \langle \sigma_x \rangle_{k=0} \quad \text{and} \quad M_s = \frac{g}{\sqrt{2}} \langle \sigma_y \rangle_{k=0}. \quad (2.12)$$

The meson screening masses can be obtained from the formulas in appendix B.

The PCAC relations determine the pion and kaon decay constants f_π, f_K from the values of the condensates [67, 80] as

$$f_\pi = \langle \sigma_x \rangle_{k=0} \quad \text{and} \quad f_K = \frac{1}{2} \langle \sigma_x \rangle_{k=0} + \frac{1}{\sqrt{2}} \langle \sigma_y \rangle_{k=0}. \quad (2.13)$$

The pressure follows from the minimum of the total effective potential at $k = 0$:

$$P_0 = - \min_{\rho_1, \rho_2} [U_{k=0}(\rho_1, \rho_2) - h_x \sigma_x - h_y \sigma_y - c_A \xi]. \quad (2.14)$$

The contribution from the pure magnetic field, $B^2/2$, is left out from our definition of the pressure, because it is independent of temperature and does not influence observables.

In addition, in the FRG method we usually include a residual term (P_r) in the total pressure P to ameliorate the ultraviolet cutoff artifacts [84–86],

$$P = P_0 - P_0|_{T=B=0} + P_r, \quad (2.15)$$

$$P_r \equiv -N_c \sum_{f=u,d,s} \sum_{s=\pm\frac{1}{2}} \sum_{n=0}^{\infty} \frac{|e_f B|}{2\pi^2} \times \\ \times \int_{\Lambda}^{\infty} dk \, \Theta(k^2 - p_{\perp}^2[e_f, s, n]) \sqrt{k^2 - p_{\perp}^2[e_f, s, n]} \left(\tanh \frac{k}{2T} - 1 \right), \quad (2.16)$$

with $p_{\perp}^2[e_f, s, n] \equiv (2n + 1 - 2s)|e_f B|$. The residual part compensates for the pressure from modes with momentum larger than Λ and ensures that the Stephan-Boltzmann limit of free quark gas is reached at sufficiently high temperatures.

From the pressure, one can extract the *bare* magnetic susceptibility $\tilde{\chi}$ as the leading response of the system to the external magnetic field:

$$P(T, B) = P(T, 0) + \frac{\tilde{\chi}(T)}{2} (eB)^2 + \mathcal{O}(B^4). \quad (2.17)$$

However, the pressure contains a B -dependent divergence and incidentally $\tilde{\chi}(T)$ is also divergent. This is related to the issue of electric charge renormalization in QED [45, 46, 48]. In this work, we renormalize $\tilde{\chi}$ by subtracting the divergent contribution at $T = 0$ as

$$\chi(T) \equiv \tilde{\chi}(T) - \tilde{\chi}(0) . \quad (2.18)$$

Thus $\chi(T = 0)$ vanishes by definition. This means that the matter contribution to the pressure at $T = 0$ begins at $\mathcal{O}(B^4)$. An intriguing consequence of renormalization is that the magnetic susceptibility obtained this way is intertwined with the nonperturbative IR physics at $T = 0$ even at arbitrarily high temperatures; this phenomenon will be demonstrated explicitly for a non-interacting gas with temperature-dependent masses in appendix D. We remark that the renormalization prescription (2.18) agrees with those in recent lattice simulations [21, 22, 24, 45, 46], hence allowing for a direct comparison between the present model calculation and the lattice data.

In actual numerics we proceed by first evaluating the subtracted pressure [21, 24]

$$\Delta P \equiv (P(T, B) - P(T, 0)) - (P(0, B) - P(0, 0)) , \quad (2.19)$$

and then measuring the magnetic susceptibility $\chi(T)$ through a polynomial fitting to ΔP .

Another important quantity that characterizes magnetic properties of the system is the magnetic permeability, μ , which is related to the magnetic susceptibility [46] as⁵

$$\mu(T) = \frac{1}{1 - 4\pi\alpha_{\text{em}} \cdot \chi(T)} . \quad (2.20)$$

Since it does not provide any new information compared to $\chi(T)$ itself, we will not show a separate plot for $\mu(T)$.

3 Numerical implementation

3.1 Setup

We solved the flow equation (2.9) with the two-dimensional Taylor method. Namely, we expand the scale-dependent effective potential around its running minimum and then cast (2.9) into a set of coupled flow equations for the coefficients of the expansion. All technical details of the Taylor method in the QM model are given in appendix C.

The flow equations for Taylor coefficients are then solved by integration from $k = \Lambda$ to $k = 0$ with the Euler method, keeping the step size of k smaller than 0.5 MeV. We confirmed numerical stability of results by changing the step size.

For the initial condition of the flow, we used

$$U_{k=\Lambda}(\rho_1, \rho_2) = a_{\Lambda}^{(1,0)} \rho_1 + \frac{a_{\Lambda}^{(2,0)}}{2} \rho_1^2 + a_{\Lambda}^{(0,1)} \rho_2 , \quad (3.1)$$

where $a_{\Lambda}^{(1,0)}$, $a_{\Lambda}^{(2,0)}$ and $a_{\Lambda}^{(0,1)}$ are free parameters of the model.

⁵In SI units, this corresponding to the ratio μ/μ_0 .

	g	$a_{\Lambda}^{(1,0)}/\Lambda^2$	$a_{\Lambda}^{(2,0)}$	$a_{\Lambda}^{(0,1)}$	h_x/Λ^3	h_y/Λ^3	c_A/Λ	f_{π}	f_K
FRG	6.5	0.56	20.0	10.0	1.76×10^{-3}	3.79×10^{-2}	4.8	91.8	112.3
MF	6.5	1.07	5.0	2.0	1.76×10^{-3}	3.79×10^{-2}	4.8	91.5	113.4

Table 1. Initial conditions at $k = \Lambda$ and the resulting f_{π} and f_K (in units of MeV) at $eB = T = 0$ for $N_f = 3$ FRG (first row) and the mean-field calculation (MF, second row). We used $\Lambda = 1$ GeV in both calculations.

particle	mass (MeV)	$ q /e$	spin	particle	mass (MeV)	$ q /e$	spin
u	298.1	2/3	1/2	s	430.8	1/3	1/2
d	298.1	1/3	1/2	—	—	—	—
π^0	138.4	0	0	a_0^0	1028.9	0	0
π^{\pm}	138.4	1	0	a_0^{\pm}	1028.9	1	0
K^0, \bar{K}^0	496.7	0	0	$\kappa^0, \bar{\kappa}^0$	1126.8	0	0
K^{\pm}	496.7	1	0	κ^{\pm}	1126.8	1	0
η	539.2	0	0	σ	533.7	0	0
η'	959.8	0	0	f_0	1237.8	0	0

Table 2. Table of quarks and mesons in the $N_f = 3$ QM model. Their masses are obtained from FRG at $eB = T = 0$ with the parameter set in Table 1.

Besides the UV cutoff scale Λ , the $N_f = 3$ QM model still has seven free parameters: $g, a_{\Lambda}^{(1,0)}, a_{\Lambda}^{(2,0)}, a_{\Lambda}^{(0,1)}, h_x, h_y$ and c_A . We adjusted these parameters so as to reproduce the pion and kaon decay constants, the light quark mass, and the pion/kaon/sigma/eta masses at $eB = T = 0$. We summarize our parameter set in Table 1 and the resulting particle masses in Table 2.

In order to evaluate the effect of mesonic fluctuations, we also performed calculations in the mean-field approximation. This is simply done by neglecting the first term in (2.9) and solving the resulting flow equation. However the initial conditions have to be readjusted to realize the same physical observables at $k = 0$; see the second row in Table 1.

In addition, we also performed FRG for the two-flavor QM model for the purpose of comparison with the three-flavor QM model. All details for the truncated effective action, the flow equation and the initial conditions are summarized in appendix A. To solve the flow equation, we again used the Taylor expansion method (see appendix C). The results from the $N_f = 2$ FRG, the $N_f = 3$ FRG and the mean-field approximation ($N_f = 3$) will be juxtaposed in section 3.2.2.

We end this subsection with a cautionary remark. The Taylor method is ineffective in the case of a first-order phase transition, because a smooth flow of the scale-dependent minimum of the potential, on which the Taylor expansion is based, breaks down. In the chiral limit, the phase transition in $U(N) \times U(N)$ -symmetric models is first order according to the one-loop ε -expansion [87], which has been confirmed by FRG with the Grid method [88–91]. Then the applicability of the Taylor method is questionable. However, as shown in [65], for physical values of the quark masses and anomaly strength, the three-flavor chiral

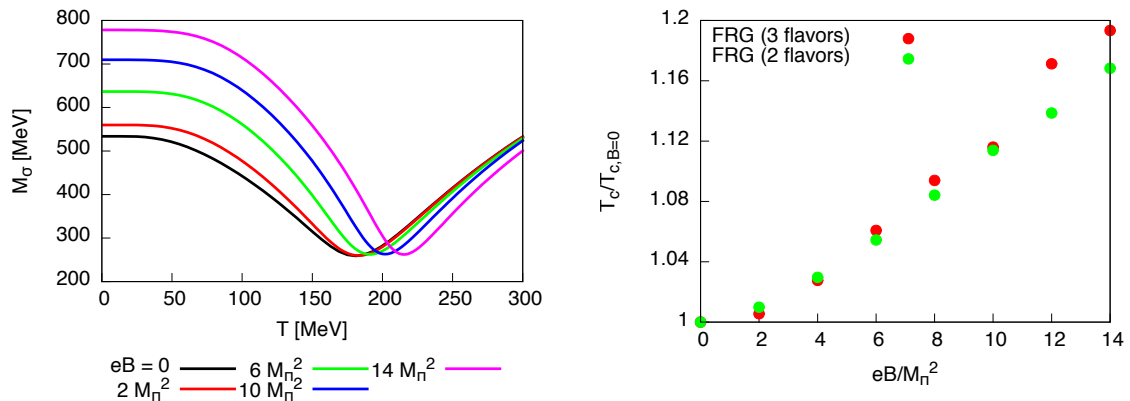


Figure 1. **Left:** The sigma meson mass from the three-flavor FRG. **Right:** Chiral pseudo-critical temperature, determined from the minimum of the sigma mass, from the two- and three-flavor FRG with a varying external magnetic field.

transition becomes a crossover at least for $B = 0$. Assuming that this is the case also for small nonzero magnetic fields, we can justify the usage of the Taylor method.

3.2 Results at nonzero magnetic field

3.2.1 Pressure, masses and decay constants

In this section we show numerical results for the particle masses, pressure, pion and kaon decay constants and the chiral pseudo-critical temperature under an external magnetic field.

In the left panel of Figure 1, we show the sigma meson mass M_σ obtained from the three-flavor FRG as a function of T across the chiral crossover. At low temperatures, M_σ increases rapidly with B . The temperature at which M_σ reaches the bottom increases from around 180 MeV at $B = 0$ to higher values for stronger B . In the right panel of Figure 1, we plot the chiral pseudo-critical temperature T_c defined as the temperature at which M_σ hits the bottom. It is found that T_c increases with B in both the two- and three-flavor FRG. Although this feature is commonly seen in almost all chiral effective models, it is at variance with lattice calculations at the physical point [15] which reports a *decrease* of T_c at least for $eB < 1 \text{ GeV}^2$. We conclude that the undesired behavior of the model cannot be cured by inclusion of fluctuations of strange quark and SU(3) mesons. We believe that T_c rising with B is not an artifact of LPA, because the inclusion of the wave function renormalization for mesons leads to an even steeper increase of T_c in the one-flavor QM model [35].

In the left panel of Figure 2, we plot the normalized pressure P/T^4 . For comparison, we display results from both the two- and three-flavor FRG calculations. At high T , the pressure slowly converges to the Stephan-Boltzmann limit of a free quark gas.⁶ At $T \lesssim 70 \text{ MeV}$ the two curves agree precisely, as expected from the fact that pions dominate the pressure at low temperatures. In the right panel of Figure 2, f_π and f_K are plotted for $eB = 0$ and $eB = 14m_\pi^2$. They increase with B at all temperatures, exhibiting the phenomenon of

⁶This behavior is due to the introduction of the residual part of the pressure (P_r) in (2.16). We found that P_r begins to matter at $T \gtrsim 200 \text{ MeV}$.

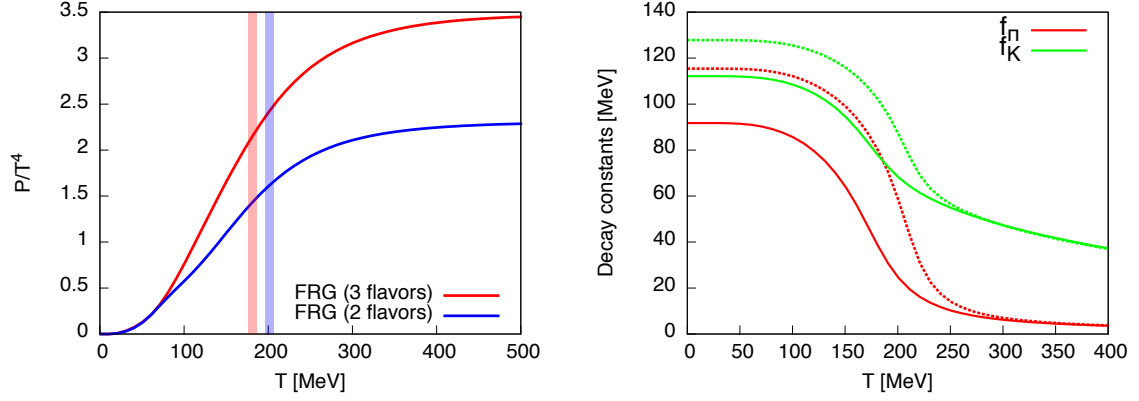


Figure 2. **Left:** Pressure from the two- and three-flavor FRG at $eB = 0$. Red and blue vertical bands indicate the pseudo-critical temperature in each theory. **Right:** The pion and kaon decay constant at finite temperature. Solid and dashed lines correspond to $eB = 0$ and $eB = 14m_\pi^2$, respectively.

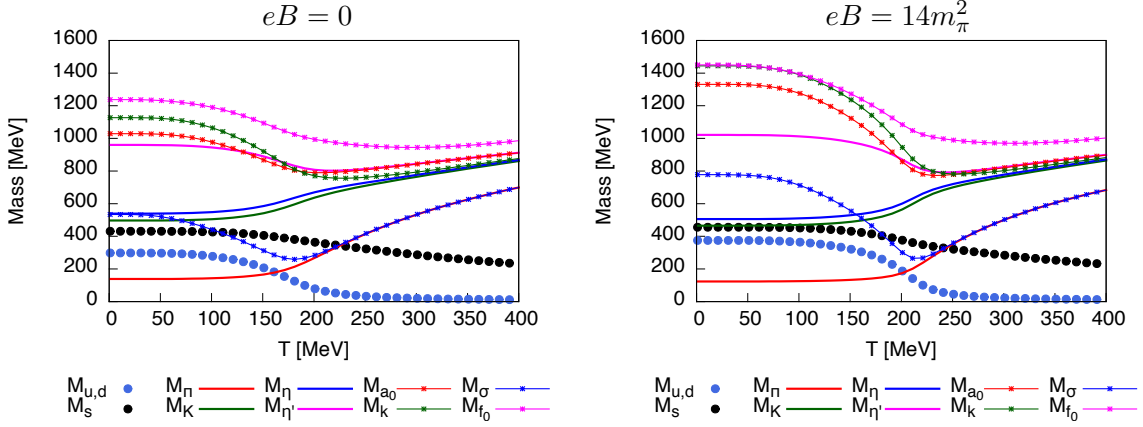


Figure 3. Masses of quarks (filled bullets), pseudo-scalar mesons (solid lines) and scalar mesons (solid lines with $*$) from the three-flavor FRG for $eB = 0$ (**Left**) and $eB = 14m_\pi^2$ (**Right**). M_k denotes the κ meson mass.

magnetic catalysis. We observe that f_K decreases very slowly compared to f_π , due to the large constituent mass of strange quark.

Figure 3 shows the quark and meson masses obtained from the three-flavor FRG calculation. The result for $eB = 0$ (left panel) is consistent with the preceding work [65]. At low temperatures, chiral symmetry is spontaneously broken and quarks acquire large dynamical masses of order $300 \sim 400$ MeV. At $T \gtrsim 180$ MeV, the light quark condensates begin to melt and sigma becomes degenerate with pions, signalling the restoration of $SU(2) \times SU(2)$ chiral symmetry. On the other hand, other mesons gain masses of order 1 GeV at high temperatures due to the large mass of strange quark. These gross features persist in the presence of a magnetic field (right panel), though the chiral crossover is shifted to a higher temperature (~ 220 MeV for $eB = 14m_\pi^2$). Note that the anomaly strength is fixed in this work: if we implement the effective restoration of $U_A(1)$ symmetry at high T , the meson

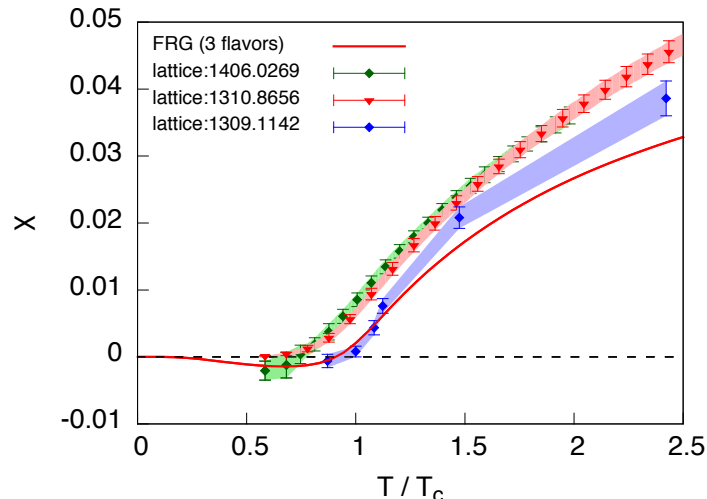


Figure 4. Magnetic susceptibility $\chi(T)$ from the three-flavor FRG calculation (solid line), in comparison with the results of lattice QCD simulations by three different groups [22, 24, 46].

spectrum would be changed qualitatively [87] but it is beyond the scope of this work.

3.2.2 Magnetic susceptibility

This section is the main part of this paper. We compare $\chi(T)$ obtained from FRG with the lattice QCD data. Although a perfect agreement with lattice cannot be expected due to the schematic nature of the QM model, we believe such a comparison could help us develop an intuitive understanding for gross features of QCD in a magnetic field.

In Figure 4, $\chi(T)$ obtained with the $N_f = 3$ FRG is plotted together with the data from three independent lattice QCD simulations [22, 24, 46].⁷ The figure shows a reasonable agreement between the FRG prediction and the lattice data over the entire temperature range. In the high- T QGP phase, quarks give a dominant paramagnetic contribution to $\chi(T)$, which is well captured by our FRG calculation. Although the shape of the curve resembles the lattice data, FRG seems to underestimate $\chi(T)$ at $T > T_c$ by about 30%. Around T_c , FRG nicely agrees with the data from [22] but disagrees with those from [24, 46]. We do not understand the origin of these discrepancies yet. One possibility is that it is somehow related to the inability of the QM model to reproduce inverse magnetic catalysis. Another possibility is that the paramagnetic contribution of spinful hadrons (e.g., ρ^\pm) which are completely ignored in the QM model has caused this discrepancy. Further investigation of this issue is left for future work.

Turning now to the hadronic phase below T_c , we observe that both FRG and the lattice data from [46] yield negative values of $\chi(T)$, which are consistent with each other within error bars. This tendency could be explained by diamagnetic contribution of light

⁷In Figure 4, the temperature is normalized by T_c at $eB = 0$: we used $T_c = 181$ MeV for the results of FRG and $T_c = 154$ MeV [92] for all the lattice data. This normalization makes a direct comparison of different methods easier.

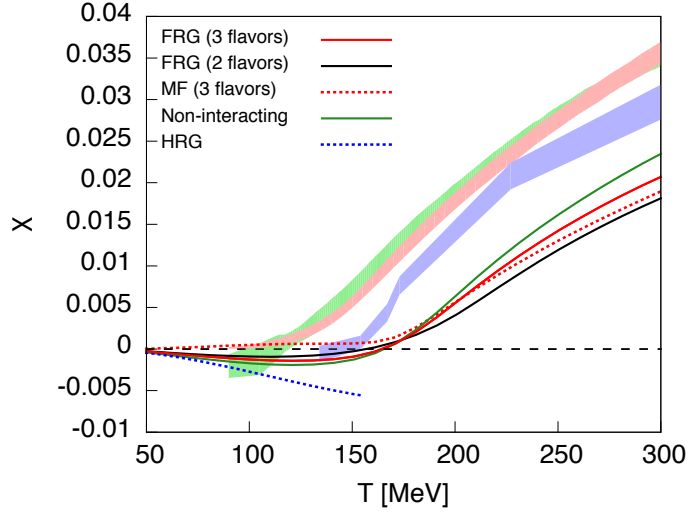


Figure 5. Magnetic susceptibilities obtained with different methods. MF and HRG denote the mean-field approximation and the Hadron Resonance Gas model, respectively. Colored bands in the figure are the same as those in Figure 4 and represent the results of lattice simulations [22, 24, 46].

pions. Indeed, the region with $\chi(T) < 0$ was not visible in the mean-field calculation of the Polyakov linear sigma model [54] which ignored meson fluctuations.

Overall, at a qualitative level, our three-flavor FRG correctly describes the transition of QCD between diamagnetism and paramagnetism in the chiral crossover. To the best of our knowledge, this is the first time such a transition is demonstrated in a strongly interacting QCD-like theory. In the future it will be important to consolidate the diamagnetic nature of QCD at low temperature by increasing lattice data points with better statistics.

In Figure 5 we showcase a collection of results from various different methods. Note that this time the horizontal axis is T (without deviation by T_c). Let us discuss characteristics of each method one by one.

1. The magnetic susceptibility obtained from the Hadron Resonance Gas (HRG) model, calculated with formulas in [46, Appendix B], is shown with a blue dashed line. It agrees with the result of FRG at $T \lesssim 70$ MeV because in this region the pressure in both calculations is dominated by light pions, which behave diamagnetically [24, 46, 48]. While $\chi(T)$ from the HRG model is monotonically decreasing for all $T < T_c$, $\chi(T)$ from FRG stops decreasing at $T \sim 130$ MeV: it is presumably because pions and kaons get heavier whereas quarks become lighter, as a result of chiral restoration in the QM model.
2. The results of two- and three-flavor FRG are shown in black and red solid lines. They share the same features ($\chi < 0$ at low T and > 0 at high T) and their difference is small over the entire temperature range. We conclude that $\chi(T)$ is rather insensitive to the inclusion of strange quark and SU(3) mesons for $T \lesssim 300$ MeV.
3. $\chi(T)$ from the mean-field approximation (MF) is plotted in a red dashed line. Not surprisingly, it is positive for all T and fails to capture the diamagnetism predicted by

FRG and HRG at low T , because MF neglects meson fluctuations altogether. This illustrates why it is imperative for the calculation of $\chi(T)$ to go beyond MF.

4. As a hybrid of FRG and the HRG model, we considered a model in which quarks and meson are non-interacting *but have temperature-dependent masses*. The magnetic susceptibility in such a model is derived in appendix D. As inputs, we inserted the masses obtained with three-flavor FRG at $eB = 0$ (shown in Figure 3). The resulting $\chi(T)$ is shown in Figure 5 as a solid green line, which mimics the results of FRG quite well at all temperatures. We conclude that the T -dependence of the mass spectrum plays a vital role in determining the behavior of $\chi(T)$.

4 Conclusions and outlook

In this work, we have investigated thermodynamic properties of a strongly interacting thermal medium under external magnetic fields. We have analysed the three-flavor quark-meson model with $U_A(1)$ anomaly, which provides a physically consistent smooth interpolation of a pion gas at low temperature and a free quark gas at high temperature. In order to go beyond the mean-field approximation we have utilized the nonperturbative functional renormalization group (FRG) equation with the local-potential approximation which enables to incorporate of fluctuations of charged and neutral mesons.

We have confirmed that within FRG the chiral pseudo-critical temperature increases with increasing external magnetic field. This is consistent with other chiral model approaches to QCD with magnetic fields but does not concur with lattice QCD simulations at the physical quark masses. We also calculated meson masses and decay constants as functions of T and eB .

We then calculated the magnetic susceptibility $\chi(T)$ in this model by extracting the $\mathcal{O}((eB)^2)$ term in the pressure, which is the main result of this paper. We found that $\chi < 0$ in the hadron phase. This is due to the fact that, at low T , pressure is dominated by the light pion contributions which render the medium weakly diamagnetic. Our result is in quantitative agreement with the lattice QCD data [46]. This diamagnetism is invisible in the mean-field approximation, because meson fluctuations are not taken into account. On the other hand, at high T , we found $\chi > 0$, whose values lie in the same ballpark as the lattice QCD outputs [21, 22, 24, 46]. This behavior is caused by chiral symmetry restoration in the QGP phase, which makes quarks lighter and mesons heavier, thereby letting the paramagnetic contribution of quarks dominate the magnetic susceptibility. We observed that $\chi(T)$ crosses zero near the pseudo-critical temperature. While such a transition between paramagnetism and diamagnetism has been known from a non-interacting MIT bag-type model [29], this work has achieved for the first time a quantitatively reliable demonstration of such a transition in a strongly interacting QCD-like model with spontaneous chiral symmetry breaking. Our results indicate that bulk features of the response of QCD to *weak* magnetic fields can be reproduced in the simple quark-meson model, even though this model does not reproduce the inverse magnetic catalysis phenomenon in a *strong* magnetic field. Understanding of the remaining 30% discrepancy of $\chi(T)$ at high

temperature between QCD and the model is an important open problem and we leave it for future work.

There are various directions to extend this work. From a technical point of view, one can systematically improve the treatment of the quark-meson model (i) by introducing a scale-dependent wave function renormalization and a flow of the Yukawa coupling g , (ii) by allowing the effective potential to depend on another invariant $\text{tr}[(\Sigma\Sigma^\dagger)^3]$, (iii) by coupling quarks to the Polyakov loop background to mimic confinement [60, 86, 93], and (iv) by making the anomaly strength c_A vary with temperature and/or magnetic field. One can also use the framework of this paper to calculate the full equation of state, magnetization, interaction measure, sound velocity, etc. with possible inclusion of a nonzero quark chemical potential. Such an extension will help to gain better understanding of the physics of compact stars and heavy ion collisions.

Acknowledgments

The authors thank G. S. Bali, G. Endrődi, T. Hatsuda and Y. Hidaka for valuable discussions. They are also grateful to useful comments from the participants of the sixth JICFuS seminar on 16 September 2014 and the workshop *RIKEN iTHES workshop on Thermal Field Theory and its applications* on 3–5 September 2014, where part of this work has been presented. KK was supported by the Special Postdoctoral Research Program of RIKEN. TK was supported by the RIKEN iTHES Project and JSPS KAKENHI Grants Number 25887014.

A Summary of the $N_f = 2$ QM model

The Lagrangian of the two-flavor QM model for $\mathbf{B} = 0$ is given by

$$\mathcal{L} = \sum_{i=1}^{N_c} \bar{\psi}_i [\not{D} + g(\sigma + i\gamma_5 \vec{\pi} \cdot \vec{\tau})] \psi_i + \frac{1}{2}(\partial_\mu \sigma)^2 + \frac{1}{2}(\partial_\mu \vec{\pi})^2 + U(\rho) - h\sigma, \quad (\text{A.1})$$

where $\psi = (u, d)^T$ denotes the two-flavor quark field with three colors ($N_c = 3$), and $\rho \equiv \sigma^2 + \vec{\pi}^2$. The last term $-h\sigma$ represents the effect of a bare quark mass. This model corresponds to the limit of infinitely strong $U_A(1)$ anomaly where η and a_0 decouple.

To calculate the effective action of the model using the FRG equation, we employ LPA. Then the Ansatz for the scale-dependent effective action with $\mathbf{B} \neq 0$ reads

$$\Gamma_k[\psi, \sigma, \pi] = \int_0^{1/T} dx_4 \int d^3x \left\{ \sum_{i=1}^{N_c} \bar{\psi}_i [\not{D} + g(\sigma + i\gamma_5 \vec{\pi} \cdot \vec{\tau})] \psi_i + \frac{1}{2}(\partial_\mu \sigma)^2 + \mathcal{D}_\mu \pi^+ \mathcal{D}_\mu \pi^- + \frac{1}{2}(\partial_\mu \pi^0)^2 + U_k(\rho) - h\sigma \right\}, \quad (\text{A.2})$$

where $\not{D} = \gamma_\mu(\partial_\mu - iQA_\mu)$ with $Q = \text{diag}(\frac{2}{3}e, -\frac{1}{3}e)$, $\mathcal{D}_\mu = \partial_\mu + ieA_\mu$, and $\pi^\pm = \frac{1}{\sqrt{2}}(\pi_1 \pm i\pi_2)$. The effect of isospin symmetry breaking by the magnetic field on the potential is neglected for simplicity. With this Ansatz and the cutoff functions (2.7a) and (2.7b), we can derive

the flow equation for the effective potential (2.9), in which the sum must now be restricted to quarks and mesons of the two-flavor QM model. The scale- and field-dependent energies that enter the flow equation are defined as

$$E_{u,d}(k) = \sqrt{k^2 + g^2 \rho}, \quad (\text{A.3a})$$

$$E_\sigma(k) = \sqrt{k^2 + 2U'_k + 4\rho U''_k}, \quad (\text{A.3b})$$

$$E_\pi(k) = \sqrt{k^2 + 2U'_k}, \quad (\text{A.3c})$$

with $U'_k \equiv \partial_\rho U_k$ and $U''_k \equiv \partial_\rho^2 U_k$. For the initial condition of the effective potential, we use

$$U_{k=\Lambda}(\rho) = a_\Lambda^{(1)} \rho + \frac{a_\Lambda^{(2)}}{2} \rho^2. \quad (\text{A.4})$$

The two-flavor QM model has four free parameters besides the UV cutoff scale Λ . We adjusted these parameters to reproduce the constituent quark mass, the sigma and pion masses and the pion decay constant $f_\pi = \langle \sigma \rangle$, as summarized in Table 3.

	g	$a_\Lambda^{(1)}/\Lambda^2$	$a_\Lambda^{(2)}$	h/Λ^3	f_π	m_π	m_σ	$M_{u,d}$
FRG ($N_f = 2$)	3.2	0.152	5.0	1.82×10^{-3}	92.5	140.3	611.3	296.1

Table 3. Initial conditions at $k = \Lambda$ and resulting observables at $k = 0$ (in units of MeV) at $eB = T = 0$ for $N_f = 2$ FRG. We used $\Lambda = 1$ GeV.

B Mass spectrum in the $N_f = 3$ QM model

In this appendix, we explicitly present the scale-dependent screening masses M_i of mesons in the three-flavor QM model, which enter the flow equation (2.9) via the scale-dependent energy $E_b(k)$. A detailed derivation of the mass matrix can be found in [65] and will not be reproduced here.

Let us switch from the strange-nonstrange basis (2.5) to a new coordinate defined by

$$X \equiv \sigma_x^2 \quad \text{and} \quad Y \equiv 2\sigma_y^2 - \sigma_x^2. \quad (\text{B.1})$$

The order parameter X parametrises the magnitude of chiral symmetry breaking in the light quark sector, whereas Y represents the SU(3) flavor symmetry breaking due to the strange quark mass. In terms of the new coordinate, the invariants may be expressed as

$$\rho_1 = \frac{3X + Y}{4} \quad \text{and} \quad \rho_2 = \frac{Y^2}{24}. \quad (\text{B.2})$$

The field-dependent squared masses $\{M_i^2\}$ of $9 + 9 = 18$ mesons are obtained as eigenvalues of the 18×18 matrix Ω_k defined by

$$(\Omega_k)_{ij} \equiv \partial_i \partial_j [U_k(\rho_1, \rho_2) - c_A \xi], \quad i, j = 1, 2, \dots, 18 \quad (\text{B.3})$$

where the derivatives are taken with respect to the meson basis $(\sigma_x, \sigma_1, \dots, \sigma_7, \sigma_y, \pi_0, \dots, \pi_8)$. We note that the explicit symmetry breaking terms $\propto h_{x,y}$ are linear in meson fields and hence do not contribute to the matrix elements of Ω_k , even though they affect the location of the minimum of the effective potential.

With the chain rule, it is tedious but straightforward to calculate the mass eigenvalues. Using the notation

$$U_k^{(i,j)}(\rho_1, \rho_2) \equiv \left(\frac{\partial}{\partial \rho_1} \right)^i \left(\frac{\partial}{\partial \rho_2} \right)^j U_k(\rho_1, \rho_2), \quad (\text{B.4})$$

we now write down the mass eigenvalues of all mesons in terms of X and Y :

- **Scalar mesons**

$$M_{a_0}^2 = U_k^{(1,0)} + \frac{6X - Y}{6} U_k^{(0,1)} + \frac{\sqrt{X+Y}}{2} c_A, \quad (\text{B.5a})$$

$$M_\kappa^2 = U_k^{(1,0)} + \frac{3X + 2Y + 3\sqrt{X}\sqrt{X+Y}}{6} U_k^{(0,1)} + \frac{\sqrt{X}}{2} c_A, \quad (\text{B.5b})$$

$$M_\sigma^2 = \frac{A_\sigma + B_\sigma + \sqrt{(A_\sigma - B_\sigma)^2 + 4C_\sigma^2}}{2}, \quad (\text{B.5c})$$

$$M_{f_0}^2 = \frac{A_\sigma + B_\sigma - \sqrt{(A_\sigma - B_\sigma)^2 + 4C_\sigma^2}}{2}, \quad (\text{B.5d})$$

with the definitions

$$A_\sigma \equiv U_k^{(1,0)} + X U_k^{(2,0)} + \frac{XY^2}{36} U_k^{(0,2)} + \frac{2X - Y}{6} U_k^{(0,1)} - \frac{YX}{3} U_k^{(1,1)} - \frac{\sqrt{X+Y}}{2} c_A, \quad (\text{B.6a})$$

$$B_\sigma \equiv U_k^{(1,0)} + \frac{X + Y}{2} U_k^{(2,0)} + \frac{(X + Y)Y^2}{18} U_k^{(0,2)} + \frac{2X + 3Y}{3} U_k^{(0,1)} + \frac{X(X + Y)}{3} U_k^{(1,1)}, \quad (\text{B.6b})$$

$$C_\sigma \equiv \frac{\sqrt{X}\sqrt{X+Y}}{\sqrt{2}} U_k^{(2,0)} - \frac{\sqrt{X}\sqrt{X+Y}Y^2}{18\sqrt{2}} U_k^{(0,2)} - \frac{2\sqrt{X}\sqrt{X+Y}}{3\sqrt{2}} U_k^{(0,1)} + \frac{\sqrt{X}\sqrt{X+Y}Y}{6\sqrt{2}} U_k^{(1,1)} - \frac{\sqrt{X}}{\sqrt{2}} c_A. \quad (\text{B.6c})$$

- **Pseudo-scalar mesons**

$$M_\pi^2 = U_k^{(1,0)} - \frac{Y}{6} U_k^{(0,1)} - \frac{\sqrt{X+Y}}{2} c_A, \quad (\text{B.7a})$$

$$M_K^2 = U_k^{(1,0)} + \frac{3X + 2Y - 3\sqrt{X}\sqrt{X+Y}}{6} U_k^{(0,1)} - \frac{\sqrt{X}}{2} c_A, \quad (\text{B.7b})$$

$$M_\eta^2 = \frac{A_\eta + B_\eta + \sqrt{(A_\eta - B_\eta)^2 + 4C_\eta^2}}{2}, \quad (\text{B.7c})$$

$$M_{\eta'}^2 = \frac{A_\eta + B_\eta - \sqrt{(A_\eta - B_\eta)^2 + 4C_\eta^2}}{2}, \quad (\text{B.7d})$$

with the definitions

$$A_\eta \equiv U_k^{(1,0)} + \frac{2\sqrt{X} + \sqrt{X+Y}}{3} c_A, \quad (\text{B.8a})$$

$$B_\eta \equiv U_k^{(1,0)} + \frac{Y}{6} U_k^{(0,1)} - \frac{4\sqrt{X} - \sqrt{X+Y}}{6} c_A, \quad (\text{B.8b})$$

$$C_\eta \equiv -\frac{Y}{3\sqrt{2}} U_k^{(0,1)} - \frac{\sqrt{X} - \sqrt{X+Y}}{3\sqrt{2}} c_A. \quad (\text{B.8c})$$

C Taylor method

The flow equation for the effective potential can be solved numerically either by a grid method or by the Taylor method. In this work we adopt the latter approach, in which the potential at a scale k is Taylor-expanded around the scale-dependent minimum. This works for any types of flow equations and is very powerful except when a strong first-order phase transition occurs. Since the chiral restoration is a smooth crossover in both two- and three-flavor QM model with physical quark masses, one can safely rely on the Taylor method to solve the flow equation. In this appendix, we derive flow equations for the Taylor coefficients of the effective potential in the two- and three-flavor QM model.

C.1 Two flavors

First we consider the flow equation in the two-flavor QM model. In this case, the potential is a function of only one variable $\rho = \sigma^2 + \vec{\pi}^2$ (recall (A.1)). Since the quark mass induces a condensate in σ -direction, we set $\vec{\pi} = \vec{0}$ so that $\sigma = \sqrt{\rho}$. Now we expand the scale-dependent effective potential around the scale dependent minimum (ρ_k),

$$\begin{aligned} \bar{U}_k(\rho) &\equiv U_k(\rho) - h\sqrt{\rho} \\ &\equiv \sum_{n=0}^{\infty} \frac{a_n}{n!} (\rho - \rho_k)^n - h\sqrt{\rho}, \end{aligned} \quad (\text{C.1})$$

where the coefficients $\{a_n\}$ are functions of k . Differentiating this expression with respect to k , we obtain an infinite family of flow equations for $\{a_n\}$,

$$\text{d}_k a_n = \partial_k U_k^{(n)} \Big|_{\rho=\rho_k} + a_{n+1} \text{d}_k \rho_k, \quad (\text{C.2})$$

with $U_k^{(n)} \equiv \partial^n U_k / \partial \rho^n$ and $\text{d}_k \equiv \frac{\text{d}}{\text{d}k}$. On the RHS, $\partial_k U_k^{(n)}$ can be obtained by differentiating the flow equation of U_k with ρ , whereas $\text{d}_k \rho_k$ may be deduced as follows: First, recall that the scale-dependent minimum of the effective potential should satisfy the following minimum condition at any scale:⁸

$$\partial_\rho \bar{U}_k \Big|_{\rho=\rho_k} \stackrel{!}{=} 0 \quad \Rightarrow \quad a_1 = \frac{h}{2\sqrt{\rho_k}} \quad \text{for } \forall k. \quad (\text{C.3})$$

⁸This minimum condition is meaningful only if the condensate is non-vanishing ($\rho_k > 0$). Fortunately, in the present work, the quark mass effect $\propto -h\sqrt{\rho}$ always guarantees a non-vanishing condensate.

Combining (C.3) with (C.2) for $n = 1$, we obtain the flow equation for the scale-dependent minimum

$$d_k \rho_k = - \frac{\partial_k U_k^{(1)}|_{\rho=\rho_k}}{\frac{h}{4\rho_k^{3/2}} + a_2}. \quad (\text{C.4})$$

In this work, we carried out the Taylor expansion up to $n = 6$.

C.2 Three flavors

Next, we consider the flow equation in the three-flavor QM model. Assuming that only σ_0 and σ_8 take nonzero values, we obtain $\Sigma = \text{diag}(\sigma_x/2, \sigma_x/2, \sigma_y/\sqrt{2})$ with $\sigma_{x,y}$ defined in (2.5). Plugging this into the definition of $\rho_{1,2}$, we find $\rho_1 = (\sigma_x^2 + \sigma_y^2)/2$ and $\frac{1}{3}\rho_1^2 + \rho_2 = (\sigma_x^4 + 2\sigma_y^4)/8$. It is then straightforward to solve them for σ_x and σ_y .

What is new for $N_f = 3$ compared to $N_f = 2$ is that the total effective potential in (2.8) is a function of *two* variables,

$$\begin{aligned} \bar{U}_k(\rho_1, \rho_2) &\equiv U_k(\rho_1, \rho_2) - h_x \sigma_x - h_y \sigma_y - c_A \xi \\ &= U_k(\rho_1, \rho_2) + f(\rho_1, \rho_2), \end{aligned} \quad (\text{C.5})$$

with

$$f(\rho_1, \rho_2) \equiv -h_x \sqrt{\frac{4\rho_1 - \sqrt{24\rho_2}}{3}} - h_y \sqrt{\frac{2\rho_1 + \sqrt{24\rho_2}}{3}} - \frac{c_A}{2\sqrt{2}} \frac{4\rho_1 - \sqrt{24\rho_2}}{3} \sqrt{\frac{2\rho_1 + \sqrt{24\rho_2}}{3}}. \quad (\text{C.6})$$

Then we have to generalize the Taylor method into two variables. The main idea is same as the two-flavor case: we expand U_k around the scale-dependent minimum $(\rho_{1,k}, \rho_{2,k})$ of \bar{U}_k as

$$U_k(\rho_1, \rho_2) = \sum_{i,j=0}^{\infty} \frac{a_{i,j}}{i!j!} (\rho_1 - \rho_{1,k})^i (\rho_2 - \rho_{2,k})^j, \quad (\text{C.7})$$

where $\{a_{i,j}\}$ are k -dependent coefficients. In this work, we take into account the coefficients up to third order of invariants, i.e., $a_{i,j}$ ($i, j \leq 3$). For convenience, let us define $\langle \mathcal{F}(\rho_1, \rho_2) \rangle_k := \mathcal{F}(\rho_{1,k}, \rho_{2,k})$ for an arbitrary function \mathcal{F} of ρ_1 and ρ_2 .

By differentiating both sides of (C.7) with respect to k we obtain an infinite tower of flow equations for the coefficients:

$$d_k a_{i,j} = \langle \partial_k U_k^{(i,j)} \rangle_k + a_{i+1,j} d_k \rho_{1,k} + a_{i,j+1} d_k \rho_{2,k}, \quad (\text{C.8})$$

with $U_k^{(i,j)}$ defined in (B.4). On the RHS, $\partial_k U_k^{(i,j)}$ can be obtained by differentiating $\partial_k U_k$ in (2.9) with respect to ρ_1 and ρ_2 , whereas $d_k \rho_{1,k}$ and $d_k \rho_{2,k}$ are derived as follows: First, the minimum condition of \bar{U}_k at $(\rho_{1,k}, \rho_{2,k})$ reads⁹

$$\langle \partial_{\rho_1} \bar{U}_k \rangle_k \stackrel{!}{=} 0 \iff a_{1,0} = -\langle \partial_{\rho_1} f \rangle_k, \quad (\text{C.9a})$$

$$\langle \partial_{\rho_2} \bar{U}_k \rangle_k \stackrel{!}{=} 0 \iff a_{0,1} = -\langle \partial_{\rho_2} f \rangle_k. \quad (\text{C.9b})$$

⁹It must be noted that these minimum conditions are meaningful only if $\rho_{1,k} > 0$ and $\rho_{2,k} > 0$. This is guaranteed for nonzero quark masses, i.e., $h_{x,y} > 0$.

By differentiating the above relations with respect to k and using (C.8), we obtain

$$a_{2,0}d_k\rho_{1,k} + a_{1,1}d_k\rho_{2,k} + \langle\partial_k U_k^{(1,0)}\rangle_k = -\langle\partial_{\rho_1}^2 f\rangle_k d_k\rho_{1,k} - \langle\partial_{\rho_1}\partial_{\rho_2}f\rangle_k d_k\rho_{2,k}, \quad (\text{C.10a})$$

$$a_{1,1}d_k\rho_{1,k} + a_{0,2}d_k\rho_{2,k} + \langle\partial_k U_k^{(0,1)}\rangle_k = -\langle\partial_{\rho_1}\partial_{\rho_2}f\rangle_k d_k\rho_{1,k} - \langle\partial_{\rho_2}^2 f\rangle_k d_k\rho_{2,k}. \quad (\text{C.10b})$$

By solving these equations for $d_k\rho_{1,k}$ and $d_k\rho_{2,k}$, we finally arrive at

$$d_k\rho_{1,k} = \frac{-\left(\langle\partial_{\rho_1}\partial_{\rho_2}f\rangle_k + a_{1,1}\right)\langle\partial_k U_k^{(0,1)}\rangle_k + \left(\langle\partial_{\rho_2}^2 f\rangle_k + a_{0,2}\right)\langle\partial_k U_k^{(1,0)}\rangle_k}{\left(\langle\partial_{\rho_1}\partial_{\rho_2}f\rangle_k + a_{1,1}\right)^2 - \left(\langle\partial_{\rho_1}^2 f\rangle_k + a_{2,0}\right)\left(\langle\partial_{\rho_2}^2 f\rangle_k + a_{0,2}\right)}, \quad (\text{C.11a})$$

$$d_k\rho_{2,k} = \frac{-\left(\langle\partial_{\rho_1}\partial_{\rho_2}f\rangle_k + a_{1,1}\right)\langle\partial_k U_k^{(1,0)}\rangle_k + \left(\langle\partial_{\rho_1}^2 f\rangle_k + a_{2,0}\right)\langle\partial_k U_k^{(0,1)}\rangle_k}{\left(\langle\partial_{\rho_1}\partial_{\rho_2}f\rangle_k + a_{1,1}\right)^2 - \left(\langle\partial_{\rho_1}^2 f\rangle_k + a_{2,0}\right)\left(\langle\partial_{\rho_2}^2 f\rangle_k + a_{0,2}\right)}. \quad (\text{C.11b})$$

D Magnetic susceptibility of a non-interacting quark-meson gas

The goal of this appendix is to derive the magnetic susceptibility of a non-interacting gas of quarks and mesons with *temperature-dependent masses*. Our new result is $\chi(T) = \chi_q(T) + \chi_m(T)$, with the contribution from quarks

$$\chi_q(T) = \frac{N_c}{6\pi^2} \sum_f \left(\frac{e_f}{e}\right)^2 \left\{ 2 \int_0^\infty \frac{dx}{\sqrt{x^2+1}} \frac{1}{\exp\left(\frac{m_f(T)}{T}\sqrt{x^2+1}\right) + 1} - \log\left(\frac{m_f(0)}{m_f(T)}\right) \right\}, \quad (\text{D.1})$$

and from charged mesons

$$\chi_m(T) = -\frac{1}{48\pi^2} \sum_b \left\{ 2 \int_0^\infty \frac{dx}{\sqrt{x^2+1}} \frac{1}{\exp\left(\frac{m_b(T)}{T}\sqrt{x^2+1}\right) - 1} + \log\left(\frac{m_b(0)}{m_b(T)}\right) \right\}, \quad (\text{D.2})$$

with T -dependent masses $m_f(T)$ and $m_b(T)$, respectively. In (D.2), the index b runs over $\pi^+, \pi^-, K^+, K^-, a_0^+, a_0^-, \kappa^+$ and κ^- . The first terms inside brackets in (D.1) and (D.2) are thermal contributions that have already been computed in [29].¹⁰ The second terms in (D.1) and (D.2) are new vacuum corrections, which we are going to work out below.

Let us begin with the vacuum energy density for a particle with spin s , charge q and mass m in a magnetic field:

$$f^{\text{vac}}(m) \equiv \mp \frac{1}{2} \sum_{n=0}^{\infty} \sum_{s_z} \frac{|qB|}{2\pi} \int \frac{dp_z}{2\pi} \sqrt{p_z^2 + m^2 + 2|qB|(n + 1/2 - s_z)}, \quad (\text{D.3})$$

where the upper sign corresponds to fermions and the lower to bosons. If m is a constant mass, then $f^{\text{vac}}(m)$ is independent of T and does not contribute to the subtracted pressure, (2.19). However this is not the case if m depends on T , as we will shortly see.

As mentioned in section 2.3, the vacuum energy density contains a B -dependent divergence that has to be regularized. We follow the renormalization scheme in [48]. With

¹⁰There is a typo in the first equation of [29, Eq.(30)]: $12\pi^2$ in the denominator should read $24\pi^2$. We checked this with a numerical software.

dimensional regularization and using dimensionless variables $a \equiv \frac{1}{2} - s_z$ and $x \equiv \frac{m^2}{2|qB|}$, we obtain (cf. [48, Eq.(3.13)])

$$\begin{aligned} & f^{\text{vac}}(m)|_{B \neq 0} - f^{\text{vac}}(m)|_{B=0} \\ &= \pm \frac{(qB)^2}{8\pi^2} \sum_a \left[\left(\frac{2}{\varepsilon} - \gamma - \log \left(\frac{2|qB|}{4\pi\mu^2} \right) + 1 \right) \left(\frac{1}{12} - \frac{a}{2} + \frac{a^2}{2} \right) - \zeta'(-1, x+a) - \frac{x^2}{4} + \frac{x^2}{2} \log x \right] \quad (\text{D.4}) \\ &=: \Delta f^{\text{vac}}(m), \end{aligned}$$

where μ is an arbitrary scale introduced for a dimensional reason. The renormalization prescription in [48] is to ensure that the quadratic term in the renormalized vacuum energy density only consists of a pure magnetic-field contribution, namely

$$\left(\Delta f^{\text{vac}}(m) + \frac{B^2}{2} \right) \Big|_{m=m_\star} \stackrel{!}{=} \frac{B_r^2}{2} + \mathcal{O}(B^4), \quad (\text{D.5})$$

where we have defined

$$B^2 = Z_q(m_\star) B_r^2, \quad q^2 = \frac{1}{Z_q(m_\star)} q_r^2, \quad \text{and} \quad q^2 B^2 = q_r^2 B_r^2, \quad (\text{D.6})$$

with the wave-function renormalization factor

$$Z_q(m_\star) \equiv 1 \mp \frac{q_r^2}{8\pi^2} \left\{ \frac{2}{\varepsilon} - \gamma - \log \left(\frac{m_\star^2}{4\pi\mu^2} \right) \right\} \sum_a \left(\frac{1}{6} - a + a^2 \right). \quad (\text{D.7})$$

Here m_\star is a fixed mass scale.

Now we are prepared to consider a T -dependent mass: $m \rightarrow m(T)$. To fulfill the condition (D.5) at $T = 0$, we must set $m_\star = m(0)$. Then, with $x = \frac{m(T)^2}{2|qB|}$ and using (D.4), we obtain

$$\begin{aligned} & \Delta f^{\text{vac}}(m(T)) + \frac{B^2}{2} \\ &= \Delta f^{\text{vac}}(m(T)) + \frac{B_r^2}{2} Z_q(m(0)) \\ &= \pm \frac{(qB)^2}{8\pi^2} \sum_a \left[\left(\frac{2}{\varepsilon} - \gamma - \log \left(\frac{2|qB|}{4\pi\mu^2} \right) + 1 \right) \left(\frac{1}{12} - \frac{a}{2} + \frac{a^2}{2} \right) - \zeta'(-1, x+a) - \frac{x^2}{4} + \frac{x^2}{2} \log x \right] \\ & \quad + \frac{B_r^2}{2} \left\{ 1 \mp \frac{q_r^2}{8\pi^2} \left\{ \frac{2}{\varepsilon} - \gamma - \log \left(\frac{m(0)^2}{4\pi\mu^2} \right) \right\} \sum_a \left(\frac{1}{6} - a + a^2 \right) \right\} \\ &= \frac{B_r^2}{2} \pm \frac{(qB)^2}{8\pi^2} \sum_a \left[\left(\log \left(\frac{m(0)^2}{2|qB|} \right) + 1 \right) \left(\frac{1}{12} - \frac{a}{2} + \frac{a^2}{2} \right) - \zeta'(-1, x+a) - \frac{x^2}{4} + \frac{x^2}{2} \log x \right]. \end{aligned}$$

In the weak field limit $x \gg 1$, we use the expansion

$$\zeta'(-1, x+a) = \frac{x^2}{2} \log x - \frac{x^2}{4} + \left(\frac{1}{12} - \frac{a}{2} + \frac{a^2}{2} \right) (\log x + 1) + \left(a - \frac{1}{2} \right) x \log x + \mathcal{O}(x^{-2})$$

and $\sum_a (a - 1/2) = 0$ to obtain

$$\begin{aligned} & \Delta f^{\text{vac}}(m(T)) + \frac{B^2}{2} \\ &= \frac{B_r^2}{2} \pm \frac{(qB)^2}{8\pi^2} \left\{ \log \left(\frac{m(0)^2}{2|qB|} \right) - \log \left(\frac{m(T)^2}{2|qB|} \right) \right\} \sum_a \left(\frac{1}{12} - \frac{a}{2} + \frac{a^2}{2} \right) + \mathcal{O}(B^4) \end{aligned} \quad (\text{D.8})$$

$$= \frac{B_r^2}{2} \pm \frac{(qB)^2}{8\pi^2} \log \left(\frac{m(0)}{m(T)} \right) \sum_a \left(\frac{1}{6} - a + a^2 \right) + \mathcal{O}(B^4). \quad (\text{D.9})$$

In the following we consider quarks and mesons separately.

D.1 Quarks

For fermions with $s = 1/2$, the sum in (D.9) over $a = 0$ and 1 is trivial and yields

$$\Delta f^{\text{vac}}(m(T)) + \frac{B^2}{2} = \frac{B_r^2}{2} + \frac{(qB)^2}{24\pi^2} \log \left(\frac{m(0)}{m(T)} \right) + \mathcal{O}(B^4). \quad (\text{D.10})$$

The total vacuum energy density of all quarks at finite T is given by

$$V_q^{\text{vac}}(T, B) \equiv -N_c \sum_f \sum_{n=0}^{\infty} \sum_{s_z} \frac{|e_f B|}{2\pi} \int \frac{dp_z}{2\pi} \sqrt{p_z^2 + m_f(T)^2 + (2n+1-2s_z)|e_f B|}. \quad (\text{D.11})$$

Comparing $V_q^{\text{vac}}(T, B)$ with (D.3) and using (D.10), we find for the total free energy

$$\frac{B^2}{2} + V_q^{\text{vac}}(T, B) - V_q^{\text{vac}}(T, 0) = \frac{B^2}{2} + 2N_c \sum_f \Delta f^{\text{vac}}(m_f(T)) \Big|_{q=e_f} \quad (\text{D.12})$$

$$= \frac{B_r^2}{2} + 2N_c \sum_f \frac{(e_f B)^2}{24\pi^2} \log \left(\frac{m_f(0)}{m_f(T)} \right) + \mathcal{O}(B^4). \quad (\text{D.13})$$

From this we obtain the vacuum correction to the magnetic susceptibility of quarks:

$$\chi_q^{\text{vac}}(T) = -\frac{N_c}{6\pi^2} \sum_f \left(\frac{e_f}{e} \right)^2 \log \left(\frac{m_f(0)}{m_f(T)} \right), \quad (\text{D.14})$$

which is nothing but the second term in (D.1).

We note in passing that, in the high-temperature limit ($T \gg m_f(T)$), the asymptotic behavior of (D.1) becomes

$$\chi_q(T) \simeq \frac{N_c}{6\pi^2} \sum_f \left(\frac{e_f}{e} \right)^2 \left\{ \log \left(\frac{T}{m_f(T)} \right) - \log \left(\frac{m_f(0)}{m_f(T)} \right) \right\} \quad (\text{D.15})$$

$$= \frac{N_c}{6\pi^2} \sum_f \left(\frac{e_f}{e} \right)^2 \log \left(\frac{T}{m_f(0)} \right) \quad (\text{D.16})$$

$$= 2\beta_1^{\text{QED}} \log \left(\frac{T}{m_f(0)} \right), \quad (\text{D.17})$$

where β_1 is the first coefficient of the QED beta function [48, 94, 95]. Interestingly, the IR divergence in the chiral limit ($m_f(T) \rightarrow 0$) neatly cancels out between the two terms in (D.15)! The final result (D.17) is well-defined and finite, if $m_f(0) > 0$ is dynamically generated. The necessity of a nonperturbative scale in the perturbative expression of magnetic susceptibility has been emphasized in [46] in the context of lattice QCD, while here we have extended their arguments to the case of a chiral effective model. It should be point out though, that the nonperturbative scale for $\chi(T)$ extracted from lattice QCD is $\Lambda_H = 120$ MeV [46], which is smaller than $m_f(0) \sim 300$ MeV by a factor of 2.5.

D.2 Mesons

For spinless bosons with charge $q = e$, (D.9) becomes

$$\Delta f^{\text{vac}}(m(T)) + \frac{B^2}{2} = \frac{B_r^2}{2} + \frac{(eB)^2}{96\pi^2} \log \left(\frac{m(0)}{m(T)} \right) + \mathcal{O}(B^4). \quad (\text{D.18})$$

The total vacuum energy density of scalar and pseudo-scalar mesons at finite T is given by

$$V_m^{\text{vac}}(T, B) \equiv \frac{1}{2} \sum_b \sum_{n=0}^{\infty} \frac{|eB|}{2\pi} \int \frac{dp_z}{2\pi} \sqrt{p_z^2 + m_b(T)^2 + (2n+1)|eB|}, \quad (\text{D.19})$$

where the index b runs over $\pi^+, \pi^-, K^+, K^-, a_0^+, a_0^-, \kappa^+$ and κ^- . Comparing $V_m^{\text{vac}}(T, B)$ with (D.3) and using (D.18), we find

$$\frac{B^2}{2} + V_m^{\text{vac}}(T, B) - V_m^{\text{vac}}(T, 0) = \frac{B^2}{2} + \sum_b \Delta f^{\text{vac}}(m_b(T)) \quad (\text{D.20})$$

$$= \frac{B_r^2}{2} + \frac{(eB)^2}{96\pi^2} \sum_b \log \left(\frac{m_b(0)}{m_b(T)} \right) + \mathcal{O}(B^4). \quad (\text{D.21})$$

From this we obtain the vacuum correction to the magnetic susceptibility of mesons:

$$\chi_m^{\text{vac}}(T) = -\frac{1}{48\pi^2} \sum_b \log \left(\frac{m_b(0)}{m_b(T)} \right), \quad (\text{D.22})$$

which is nothing but the second term in (D.2).

References

- [1] R. C. Duncan and C. Thompson, *Formation of very strongly magnetized neutron stars - implications for gamma-ray bursts*, *Astrophys.J.* **392** (1992) L9.
- [2] A. K. Harding and D. Lai, *Physics of Strongly Magnetized Neutron Stars*, *Rept.Prog.Phys.* **69** (2006) 2631, [[astro-ph/0606674](#)].
- [3] D. Grasso and H. R. Rubinstein, *Magnetic fields in the early universe*, *Phys.Rept.* **348** (2001) 163–266, [[astro-ph/0009061](#)].
- [4] D. E. Kharzeev, L. D. McLerran, and H. J. Warringa, *The Effects of topological charge change in heavy ion collisions: 'Event by event P and CP violation'*, *Nucl.Phys.* **A803** (2008) 227–253, [[arXiv:0711.0950](#)].

- [5] K. Fukushima, D. E. Kharzeev, and H. J. Warringa, *The Chiral Magnetic Effect*, *Phys. Rev.* **D78** (2008) 074033, [[arXiv:0808.3382](#)].
- [6] V. Skokov, A. Y. Illarionov, and V. Toneev, *Estimate of the magnetic field strength in heavy-ion collisions*, *Int.J.Mod.Phys.* **A24** (2009) 5925–5932, [[arXiv:0907.1396](#)].
- [7] R. Gatto and M. Ruggieri, *Quark Matter in a Strong Magnetic Background*, *Lect.Notes Phys.* **871** (2013) 87–119, [[arXiv:1207.3190](#)].
- [8] I. A. Shovkovy, *Magnetic Catalysis: A Review*, *Lect.Notes Phys.* **871** (2013) 13–49, [[arXiv:1207.5081](#)].
- [9] V. Gusynin, V. Miransky, and I. Shovkovy, *Dimensional reduction and dynamical chiral symmetry breaking by a magnetic field in (3+1)-dimensions*, *Phys.Lett.* **B349** (1995) 477–483, [[hep-ph/9412257](#)].
- [10] V. Gusynin, V. Miransky, and I. Shovkovy, *Dimensional reduction and catalysis of dynamical symmetry breaking by a magnetic field*, *Nucl.Phys.* **B462** (1996) 249–290, [[hep-ph/9509320](#)].
- [11] P. Buividovich, M. Chernodub, E. Luschevskaya, and M. Polikarpov, *Numerical study of chiral symmetry breaking in non-Abelian gauge theory with background magnetic field*, *Phys.Lett.* **B682** (2010) 484–489, [[arXiv:0812.1740](#)].
- [12] M. D’Elia, S. Mukherjee, and F. Sanfilippo, *QCD Phase Transition in a Strong Magnetic Background*, *Phys.Rev.* **D82** (2010) 051501, [[arXiv:1005.5365](#)].
- [13] M. D’Elia and F. Negro, *Chiral Properties of Strong Interactions in a Magnetic Background*, *Phys.Rev.* **D83** (2011) 114028, [[arXiv:1103.2080](#)].
- [14] V. Braguta, P. Buividovich, M. Chernodub, A. Y. Kotov, and M. Polikarpov, *Electromagnetic superconductivity of vacuum induced by strong magnetic field: numerical evidence in lattice gauge theory*, *Phys.Lett.* **B718** (2012) 667–671, [[arXiv:1104.3767](#)].
- [15] G. Bali, F. Bruckmann, G. Endrodi, Z. Fodor, S. Katz, et al., *The QCD phase diagram for external magnetic fields*, *JHEP* **1202** (2012) 044, [[arXiv:1111.4956](#)].
- [16] E.-M. Ilgenfritz, M. Kalinowski, M. Muller-Preussker, B. Petersson, and A. Schreiber, *Two-color QCD with staggered fermions at finite temperature under the influence of a magnetic field*, *Phys.Rev.* **D85** (2012) 114504, [[arXiv:1203.3360](#)].
- [17] E. Luschevskaya and O. Larina, *The ρ and a mesons in a strong abelian magnetic field in $SU(2)$ lattice gauge theory*, [arXiv:1203.5699](#).
- [18] G. Bali, F. Bruckmann, G. Endrodi, Z. Fodor, S. Katz, et al., *QCD quark condensate in external magnetic fields*, *Phys.Rev.* **D86** (2012) 071502, [[arXiv:1206.4205](#)].
- [19] G. Bali, F. Bruckmann, M. Constantinou, M. Costa, G. Endrodi, et al., *Magnetic susceptibility of QCD at zero and at finite temperature from the lattice*, *Phys.Rev.* **D86** (2012) 094512, [[arXiv:1209.6015](#)].
- [20] G. Bali, F. Bruckmann, G. Endrodi, F. Gruber, and A. Schaefer, *Magnetic field-induced gluonic (inverse) catalysis and pressure (an)isotropy in QCD*, *JHEP* **1304** (2013) 130, [[arXiv:1303.1328](#)].
- [21] C. Bonati, M. D’Elia, M. Mariti, F. Negro, and F. Sanfilippo, *Magnetic Susceptibility of Strongly Interacting Matter across the Deconfinement Transition*, *Phys.Rev.Lett.* **111** (2013) 182001, [[arXiv:1307.8063](#)].

- [22] L. Levkova and C. DeTar, *Quark-gluon plasma in an external magnetic field*, *Phys.Rev.Lett.* **112** (2014) 012002, [[arXiv:1309.1142](#)].
- [23] E. M. Ilgenfritz, M. Muller-Preussker, B. Petersson, and A. Schreiber, *Magnetic catalysis (and inverse catalysis) at finite temperature in two-color lattice QCD*, *Phys.Rev.* **D89** (2014) 054512, [[arXiv:1310.7876](#)].
- [24] C. Bonati, M. D’Elia, M. Mariti, F. Negro, and F. Sanfilippo, *Magnetic susceptibility and equation of state of $N_f = 2 + 1$ QCD with physical quark masses*, *Phys.Rev.* **D89** (2014) 054506, [[arXiv:1310.8656](#)].
- [25] V. Bornyakov, P. Buividovich, N. Cundy, O. Kochetkov, and A. Schafer, *Deconfinement transition in two-flavour lattice QCD with dynamical overlap fermions in an external magnetic field*, *Phys.Rev.* **D90** (2014) 034501, [[arXiv:1312.5628](#)].
- [26] M. D’Elia, *Lattice QCD Simulations in External Background Fields*, *Lect.Notes Phys.* **871** (2013) 181–208, [[arXiv:1209.0374](#)].
- [27] F. Preis, A. Rebhan, and A. Schmitt, *Inverse magnetic catalysis in dense holographic matter*, *JHEP* **1103** (2011) 033, [[arXiv:1012.4785](#)].
- [28] F. Preis, A. Rebhan, and A. Schmitt, *Inverse magnetic catalysis in field theory and gauge-gravity duality*, *Lect.Notes Phys.* **871** (2013) 51–86, [[arXiv:1208.0536](#)].
- [29] N. Agasian and S. Fedorov, *Quark-hadron phase transition in a magnetic field*, *Phys.Lett.* **B663** (2008) 445–449, [[arXiv:0803.3156](#)].
- [30] E. S. Fraga and L. F. Palhares, *Deconfinement in the presence of a strong magnetic background: an exercise within the MIT bag model*, *Phys.Rev.* **D86** (2012) 016008, [[arXiv:1201.5881](#)].
- [31] K. Fukushima and Y. Hidaka, *Magnetic Catalysis vs Magnetic Inhibition*, *Phys.Rev.Lett.* **110** (2013) 031601, [[arXiv:1209.1319](#)].
- [32] F. Bruckmann, G. Endrodi, and T. G. Kovacs, *Inverse magnetic catalysis and the Polyakov loop*, *JHEP* **1304** (2013) 112, [[arXiv:1303.3972](#)].
- [33] J. Chao, P. Chu, and M. Huang, *Inverse magnetic catalysis induced by sphalerons*, *Phys.Rev.* **D88** (2013) 054009, [[arXiv:1305.1100](#)].
- [34] E. Fraga, B. Mintz, and J. Schaffner-Bielich, *A search for inverse magnetic catalysis in thermal quark-meson models*, *Phys.Lett.* **B731** (2014) 154–158, [[arXiv:1311.3964](#)].
- [35] K. Kamikado and T. Kanazawa, *Chiral dynamics in a magnetic field from the functional renormalization group*, *JHEP* **1403** (2014) 009, [[arXiv:1312.3124](#)].
- [36] R. Farias, K. Gomes, G. Krein, and M. Pinto, *The Importance of Asymptotic Freedom for the Pseudocritical Temperature in Magnetized Quark Matter*, [[arXiv:1404.3931](#)].
- [37] M. Ferreira, P. Costa, O. Lourenco, T. Frederico, and C. Providencia, *Inverse magnetic catalysis in the $(2+1)$ -flavor Nambu–Jona-Lasinio and Polyakov–Nambu–Jona-Lasinio models*, *Phys.Rev.* **D89** (2014) 116011, [[arXiv:1404.5577](#)].
- [38] A. Ayala, M. Loewe, A. J. Mizher, and R. Zamora, *Inverse magnetic catalysis for the chiral transition induced by thermo-magnetic effects on the coupling constant*, *Phys.Rev.* **D90** (2014) 036001, [[arXiv:1406.3885](#)].
- [39] A. Ayala, M. Loewe, and R. Zamora, *Anticatalysis in the linear sigma model with quarks*, [[arXiv:1406.7408](#)].

- [40] E. Ferrer, V. de la Incera, and X. Wen, *Quark Antiscreening at Strong Magnetic Field and Inverse Magnetic Catalysis*, [arXiv:1407.3503](#).
- [41] S. Fayazbakhsh and N. Sadooghi, *Anomalous magnetic moment of hot quarks, inverse magnetic catalysis and reentrance of chiral symmetry broken phase*, [arXiv:1408.5457](#).
- [42] B. Ioffe and A. V. Smilga, *Nucleon Magnetic Moments and Magnetic Properties of Vacuum in QCD*, *Nucl.Phys.* **B232** (1984) 109.
- [43] P. Buividovich, M. Chernodub, E. Luschevskaya, and M. Polikarpov, *Chiral magnetization of non-Abelian vacuum: A Lattice study*, *Nucl.Phys.* **B826** (2010) 313–327, [[arXiv:0906.0488](#)].
- [44] M. Frasca and M. Ruggieri, *Magnetic Susceptibility of the Quark Condensate and Polarization from Chiral Models*, *Phys.Rev.* **D83** (2011) 094024, [[arXiv:1103.1194](#)].
- [45] G. Bali, F. Bruckmann, G. Endrodi, and A. Schafer, *Paramagnetic squeezing of QCD matter*, *Phys.Rev.Lett.* **112** (2014) 042301, [[arXiv:1311.2559](#)].
- [46] G. Bali, F. Bruckmann, G. Endrodi, S. Katz, and A. Schaefer, *The QCD equation of state in background magnetic fields*, *JHEP* **1408** (2014) 177, [[arXiv:1406.0269](#)].
- [47] T. D. Cohen and E. S. Werbos, *Magnetization of the QCD vacuum at large fields*, *Phys.Rev.* **C80** (2009) 015203, [[arXiv:0810.5103](#)].
- [48] G. Endrodi, *QCD equation of state at nonzero magnetic fields in the Hadron Resonance Gas model*, *JHEP* **1304** (2013) 023, [[arXiv:1301.1307](#)].
- [49] O. Bergman, G. Lifschytz, and M. Lippert, *Response of Holographic QCD to Electric and Magnetic Fields*, *JHEP* **0805** (2008) 007, [[arXiv:0802.3720](#)].
- [50] T. Steinert and W. Cassing, *Electric and magnetic response of hot QCD matter*, *Phys.Rev.* **C89** (2014) 035203, [[arXiv:1312.3189](#)].
- [51] D. N. Kabat, K.-M. Lee, and E. J. Weinberg, *QCD vacuum structure in strong magnetic fields*, *Phys.Rev.* **D66** (2002) 014004, [[hep-ph/0204120](#)].
- [52] V. Orlovsky and Y. A. Simonov, *Magnetic susceptibility in QCD*, [arXiv:1405.2697](#).
- [53] M. M. Anber and M. Unsal, *QCD in magnetic field, Landau levels and double-life of unbroken center-symmetry*, [arXiv:1309.4394](#).
- [54] A. N. Tawfik and N. Magdy, *SU(3) Polyakov Linear Sigma-Model in an External Magnetic Field*, *Phys.Rev.* **C90** (2014) 015204, [[arXiv:1406.7488](#)].
- [55] C. Wetterich, *Exact evolution equation for the effective potential*, *Phys.Lett.* **B301** (1993) 90–94.
- [56] J. Berges, N. Tetradis, and C. Wetterich, *Nonperturbative renormalization flow in quantum field theory and statistical physics*, *Phys.Rept.* **363** (2002) 223–386, [[hep-ph/0005122](#)].
- [57] J. M. Pawłowski, *Aspects of the functional renormalisation group*, *Annals Phys.* **322** (2007) 2831–2915, [[hep-th/0512261](#)].
- [58] B. Delamotte, *An Introduction to the nonperturbative renormalization group*, *Lect.Notes Phys.* **852** (2012) 49–132, [[cond-mat/0702365](#)].
- [59] J. Braun, *Fermion Interactions and Universal Behavior in Strongly Interacting Theories*, *J.Phys.* **G39** (2012) 033001, [[arXiv:1108.4449](#)].
- [60] V. Skokov, *Phase diagram in an external magnetic field beyond a mean-field approximation*, *Phys.Rev.* **D85** (2012) 034026, [[arXiv:1112.5137](#)].

- [61] D. D. Scherer and H. Gies, *Renormalization Group Study of Magnetic Catalysis in the 3d Gross-Neveu Model*, *Phys.Rev.* **B85** (2012) 195417, [[arXiv:1201.3746](#)].
- [62] K. Fukushima and J. M. Pawłowski, *Magnetic catalysis in hot and dense quark matter and quantum fluctuations*, *Phys.Rev.* **D86** (2012) 076013, [[arXiv:1203.4330](#)].
- [63] J. O. Andersen and A. Tranberg, *The Chiral transition in a magnetic background: Finite density effects and the functional renormalization group*, *JHEP* **1208** (2012) 002, [[arXiv:1204.3360](#)].
- [64] J. O. Andersen, W. R. Naylor, and A. Tranberg, *Chiral and deconfinement transitions in a magnetic background using the functional renormalization group with the Polyakov loop*, *JHEP* **1404** (2014) 187, [[arXiv:1311.2093](#)].
- [65] M. Mitter and B.-J. Schaefer, *Fluctuations and the axial anomaly with three quark flavors*, *Phys.Rev.* **D89** (2014) 054027, [[arXiv:1308.3176](#)].
- [66] D. Jungnickel and C. Wetterich, *Effective action for the chiral quark-meson model*, *Phys.Rev.* **D53** (1996) 5142–5175, [[hep-ph/9505267](#)].
- [67] B.-J. Schaefer and M. Wagner, *The Three-flavor chiral phase structure in hot and dense QCD matter*, *Phys.Rev.* **D79** (2009) 014018, [[arXiv:0808.1491](#)].
- [68] B.-J. Schaefer, M. Wagner, and J. Wambach, *Thermodynamics of (2+1)-flavor QCD: Confronting Models with Lattice Studies*, *Phys.Rev.* **D81** (2010) 074013, [[arXiv:0910.5628](#)].
- [69] S. Chatterjee and K. A. Mohan, *Including the Fermion Vacuum Fluctuations in the (2 + 1) flavor Polyakov Quark Meson Model*, *Phys.Rev.* **D85** (2012) 074018, [[arXiv:1108.2941](#)].
- [70] B. Schaefer and M. Wagner, *QCD critical region and higher moments for three flavor models*, *Phys.Rev.* **D85** (2012) 034027, [[arXiv:1111.6871](#)].
- [71] B. W. Mintz, R. Stiele, R. O. Ramos, and J. Schaffner-Bielich, *Phase diagram and surface tension in the three-flavor Polyakov-quark-meson model*, *Phys.Rev.* **D87** (2013), no. 3 036004, [[arXiv:1212.1184](#)].
- [72] R. Stiele, E. S. Fraga, and J. Schaffner-Bielich, *Thermodynamics of (2+1)-flavor strongly interacting matter at nonzero isospin*, *Phys.Lett.* **B729** (2014) 72–78, [[arXiv:1307.2851](#)].
- [73] T. Beisitzer, R. Stiele, and J. Schaffner-Bielich, *Supernova Equation of State with an extended $SU(3)$ Quark-Meson Model*, [[arXiv:1403.8011](#)].
- [74] M. Levy, *Currents and Symmetry Breaking*, *Nuovo Cimento* **52** (1967) 23–49.
- [75] S. Gasiorowicz and D. Geffen, *Effective Lagrangians and field algebras with chiral symmetry*, *Rev.Mod.Phys.* **41** (1969) 531–573.
- [76] J. Schechter and Y. Ueda, *Symmetry breaking and spin-zero mass spectrum*, *Phys.Rev.* **D3** (1971) 168–176.
- [77] J. Schechter and Y. Ueda, *General treatment of the breaking of chiral symmetry and scale invariance in the $SU(3)$ sigma model*, *Phys.Rev.* **D3** (1971) 2874–2893.
- [78] L.-H. Chan and R. W. Haymaker, *Meson Dynamics in the $SU(3) \times SU(3)$ Sigma Model*, *Phys.Rev.* **D10** (1974) 4143.
- [79] M. Napsuciale, *Scalar meson masses and mixing angle in a $U(3) \times U(3)$ linear sigma model*, [[hep-ph/9803396](#)].

- [80] J. T. Lenaghan, D. H. Rischke, and J. Schaffner-Bielich, *Chiral symmetry restoration at nonzero temperature in the $SU(3)(r) \times SU(3)(l)$ linear sigma model*, *Phys.Rev.* **D62** (2000) 085008, [[nucl-th/0004006](#)].
- [81] D. Roder, J. Ruppert, and D. H. Rischke, *Chiral symmetry restoration in linear sigma models with different numbers of quark flavors*, *Phys.Rev.* **D68** (2003) 016003, [[nucl-th/0301085](#)].
- [82] D. Parganlija, P. Kovacs, G. Wolf, F. Giacosa, and D. H. Rischke, *Meson vacuum phenomenology in a three-flavor linear sigma model with (axial-)vector mesons*, *Phys.Rev.* **D87** (2013) 014011, [[arXiv:1208.0585](#)].
- [83] D. F. Litim, *Optimized renormalization group flows*, *Phys.Rev.* **D64** (2001) 105007, [[hep-th/0103195](#)].
- [84] J. Braun, K. Schwenzer, and H.-J. Pirner, *Linking the quark meson model with QCD at high temperature*, *Phys.Rev.* **D70** (2004) 085016, [[hep-ph/0312277](#)].
- [85] J. Braun, *Thermodynamics of QCD low-energy models and the derivative expansion of the effective action*, *Phys.Rev.* **D81** (2010) 016008, [[arXiv:0908.1543](#)].
- [86] T. K. Herbst, J. M. Pawłowski, and B.-J. Schaefer, *The phase structure of the Polyakov-quark-meson model beyond mean field*, *Phys.Lett.* **B696** (2011) 58–67, [[arXiv:1008.0081](#)].
- [87] R. D. Pisarski and F. Wilczek, *Remarks on the Chiral Phase Transition in Chromodynamics*, *Phys.Rev.* **D29** (1984) 338–341.
- [88] J. Berges and C. Wetterich, *Equation of state and coarse grained free energy for matrix models*, *Nucl.Phys.* **B487** (1997) 675–720, [[hep-th/9609019](#)].
- [89] J. Berges, N. Tetradis, and C. Wetterich, *Coarse graining and first order phase transitions*, *Phys.Lett.* **B393** (1997) 387–394, [[hep-ph/9610354](#)].
- [90] K. Fukushima, K. Kamikado, and B. Klein, *Second-order and Fluctuation-induced First-order Phase Transitions with Functional Renormalization Group Equations*, *Phys.Rev.* **D83** (2011) 116005, [[arXiv:1010.6226](#)].
- [91] G. Fejos, *Fluctuation induced first order phase transition in $U(n) \times U(n)$ models using chiral invariant expansion of FRG flows*, [arXiv:1409.3695](#).
- [92] A. Bazavov, T. Bhattacharya, M. Cheng, C. DeTar, H. Ding, et al., *The chiral and deconfinement aspects of the QCD transition*, *Phys.Rev.* **D85** (2012) 054503, [[arXiv:1111.1710](#)].
- [93] V. Skokov, B. Stokic, B. Friman, and K. Redlich, *Meson fluctuations and thermodynamics of the Polyakov loop extended quark-meson model*, *Phys.Rev.* **C82** (2010) 015206, [[arXiv:1004.2665](#)].
- [94] P. Elmfors, D. Persson, and B.-S. Skagerstam, *QED effective action at finite temperature and density*, *Phys.Rev.Lett.* **71** (1993) 480–483, [[hep-th/9305004](#)].
- [95] P. Elmfors, D. Persson, and B.-S. Skagerstam, *Real time thermal propagators and the QED effective action for an external magnetic field*, *Astropart.Phys.* **2** (1994) 299–326, [[hep-ph/9312226](#)].